CARBON XXX (2013) XXX–XXX

Available at www.sciencedirect.com

SciVerse ScienceDirect

journal homepage: www.elsevier.com/locate/carbon

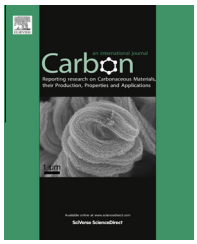

Review

Impermeability of graphene and its applications

Vikas Berry *

Department of Chemical Engineering, Kansas State University, 1005 Durland Hall, Manhattan, KS 66506, USA

ARTICLE INFO

Article history:
Received 2 April 2013
Accepted 26 May 2013
Available online xxxx

ABSTRACT

This review discusses the genesis of impermeability in graphene and its extraordinary applications in fluid-encasement for wet electron-microscopy, selective gas-permeation, nanopore-bio-diffusion, and barrier coating against rusting and environmental hazards. As the thinnest material, graphene is composed of sp^2 hybridized carbon atoms linked to one another in a 2D honeycomb lattice with high electron-density in its aromatic rings, which blocks-off all molecules. This phenomena, in combination with its strong structure (C–C bond energy = 4.9 eV and intrinsic strength = 43 N/m) makes graphene the most impermeable membrane (thinnest membrane that is impermeable). Apart from the applications mentioned above, graphene coatings have enabled fundamental studies on chemical processes and fluid structures. For example, graphene can allow electron imaging of nanocrystal nucleation process and water-lattice-structure due to its impermeability. Along with being the strongest, most conductive, and optically-absorbing material (~2.3% optical absorbance), graphene's impermeability opens a wide range of exciting opportunities.

Contents

1. Introduction

Graphene – a single atom thick sheet of sp^2 hybridized carbon atoms arranged in honeycomb lattice – is the thinnest 2D material (Fig. 1) [9]. Graphene's overlapping π-orbitals with large scattering length imparts it with a high room-temperature mobility [13–16]. Furthermore, it exhibits high optical absorptivity (2.3%) [17], high thermal conductivity (25× silicon)

* Fax: +1 785 532 7372.
E-mail address: vberry@ksu.edu.

0008-6223/$ - see front matter
http://dx.doi.org/10.1016/j.carbon.2013.05.052

Please cite this article in press as: Berry V. Impermeability of graphene and its applications. Carbon (2013), http://dx.doi.org/10.1016/j.carbon.2013.05.052

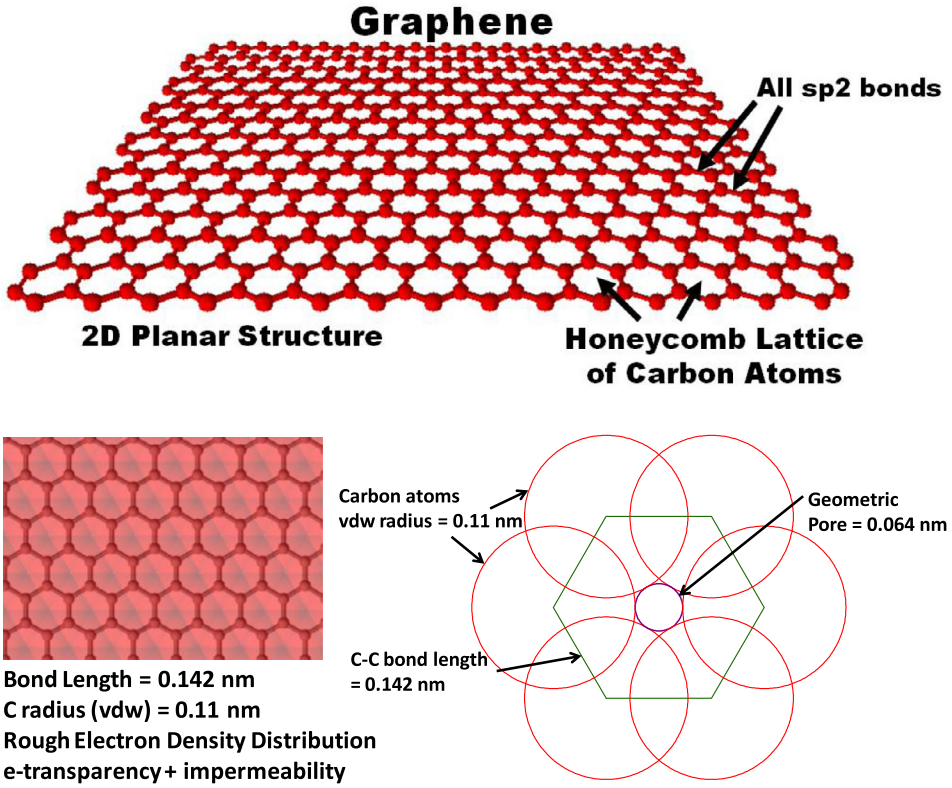

Fig. 1 – Graphene lattice structure: sp^2 hybridized carbon atoms arranged in a 2D honeycomb lattice. (Bottom) the molecular structure with rough electronic density distribution: while graphene is relatively transparent to electrons, it is practically impermeable to all molecules at room temperature. Geometric pore (0.064 nm) is also small enough not to allow molecules to pass through.

[18], and high mechanical strength (strongest nanomaterial) [19]. It has been used in several extraordinary applications, including ultrafast photo-detectors [20], single molecule detectors [21,22], ultrafast FETs [14,23–25], single-bacterial/DNA detectors [26], hydrogen visualization-templates for TEM [27], and tunable spintronic [28–30] devices. Further, it possesses a unique electronic structure [31,32], which can be controlled chemically [33,34] and geometrically [35].

Although it is only one atom thick, an interesting property of graphene is its impermeability. Graphene's π-orbitals forms a dense [36], delocalized cloud that blocks the gap within its aromatic rings (Fig. 1). This creates a repelling field, which does not allow even the smallest molecules, like hydrogen and helium, to pass through even when ~1–5 atm pressure difference is imposed across its atomic thickness at room temperature [4]. The ability to withstand such pressure differences (6 atm) in graphene is a result of its high strength (breaking strength = 42 N/m) and Young's modulus (1 TPa) [19], which retains the structural integrity of graphene. While the theoretical studies have shown that there is no gap in electron-density around the aromatic rings to allow molecules to pass, it can be seen the geometric gap calculated from van der Waals (vdw) radius of carbon will be smaller than the size of He (Fig. 1). The C–C bond length [13] of 0.142 nm in graphene implies that considering the nuclei alone, the pore size would be 0.246 nm. Now if we add the vdw radius of carbon of 0.11 nm, this geometric pore size would decrease to 0.064 nm. This geometric gap is smaller than the vdw diameter of small molecules like helium and hydrogen: 0.28 nm and 0.314 nm (bond-length (0.074 nm) + 2*r* (0.12 nm)), respectively.

Since the permeance of a membrane ($Q = \text{flux}/(\Delta P) = C.Pr/(\Delta P)$, where C, Pr and ΔP are the particle collision rate $\left(c = \frac{\rho}{4}\sqrt{\frac{8kT}{\pi m}}\right)$, the probability of diffusion (Pr) and pressure difference (ΔP), respectively, increases with reduction in the membrane thickness, and graphene is the thinnest 2D material, along with the fact that it does not allow any molecule to pass through, it can safely be graded as the most impermeable material. Via a similar argument, graphene with controlled pores can form the ultimate thin membrane for gas separation or fluid purification. This property is gaining attention since it has already shown a wide range of applications, as discussed in this review. Further, other properties of graphene can be combined with its impermeability to develop corresponding applications. For example, the flexible [37] and stretchable [19] carbon–carbon bonds in graphene can allow conformal coating on corrugated surfaces to make them impermeable [12]. The high electron-transparency and conformability can be employed to construct atomically-thin impermeable liquid cells for transmission electron microscope (TEM) imaging. The strength of graphene to withstand high pressure difference and its high electrical conductivity enables liquid retention and reduction in electrical charging during electron-microscopy imaging. Moreover, chemical interfaces of graphene with membranes can be used to control its permeance, and it can be used as a protective coating

Please cite this article in press as: Berry V. Impermeability of graphene and its applications. Carbon (2013), http://dx.doi.org/10.1016/j.carbon.2013.05.052

to prevent metal-corrosion and to quarantine hazardous nanomaterials. The next section will discuss the impermeability of graphene, followed by its applications.

2. Impermeability of graphene

Bunch et al. tested the permeance of several gases through a micro-chamber capped with a graphene sheet [4] (Fig. 2). Here, the graphene sheet blister depresses and stretches under a negative pressure difference of −93 kPa across the monolayer sheet (on a 2 × 2 μm^2 hole) by applying vacuum (0.1 Pa) for 4 days and releasing the system to atmospheric pressure of different gases. The leak rate values are calculated by measuring the pressure change:

$$\frac{dN}{dt} = \frac{V}{k_B T}\frac{dP}{dt} \quad (1)$$

For He, a leak rate of 10^5–10^6 atoms/s is measured for the chamber; this rate does not change with number of graphene layers. Importantly, estimated diffusion through the silica microchamber yields similar leak rate. This implies that the permeation is not through the graphene sheet, but through the microchamber walls. Further, Bunch et al. also estimated the upper bound of the probability of transmittance of a He atom through graphene ($\frac{dN}{dt}\frac{2d}{Nv}$, where d is the depth of the microchamber and v is the velocity of He atom) to be 10^{-11}. With estimated tunneling barrier [38] of 8 eV [39] (or 3.5 eV for the temporary bond-breaking 'window' mechanism [40]) for He transmittance through graphene, the probability of transmittance of He is orders of magnitude lower at 10^{-335} (or 10^{-212}):

$$p = \exp\left(\frac{-2x\sqrt{2m(V-E)}}{\hbar}\right) \quad (2)$$

where x = 0.3 nm, V is 8 eV (or 3.5 eV), and E is 25 meV (room temperature). Therefore, for all practical purposes, graphene is impermeable [41,42]. Further, the permeance of graphene is related with the route of its synthesis, since it influences the defects on graphene. For example, CVD graphene is expected to have Stone–Wales defects, which reduce the barrier to He diffusion. Although, this reduction in barrier height (calculated to be between 6 and 9.2 eV) is not sufficient to allow ready passage of He [38]. However, other defects can significantly reduce the barrier to He penetration, as per calculations; for example vacancy defects 555777 divacancy, 858 divacancy, tetravacancy, hexavacancy, and decavancy induce

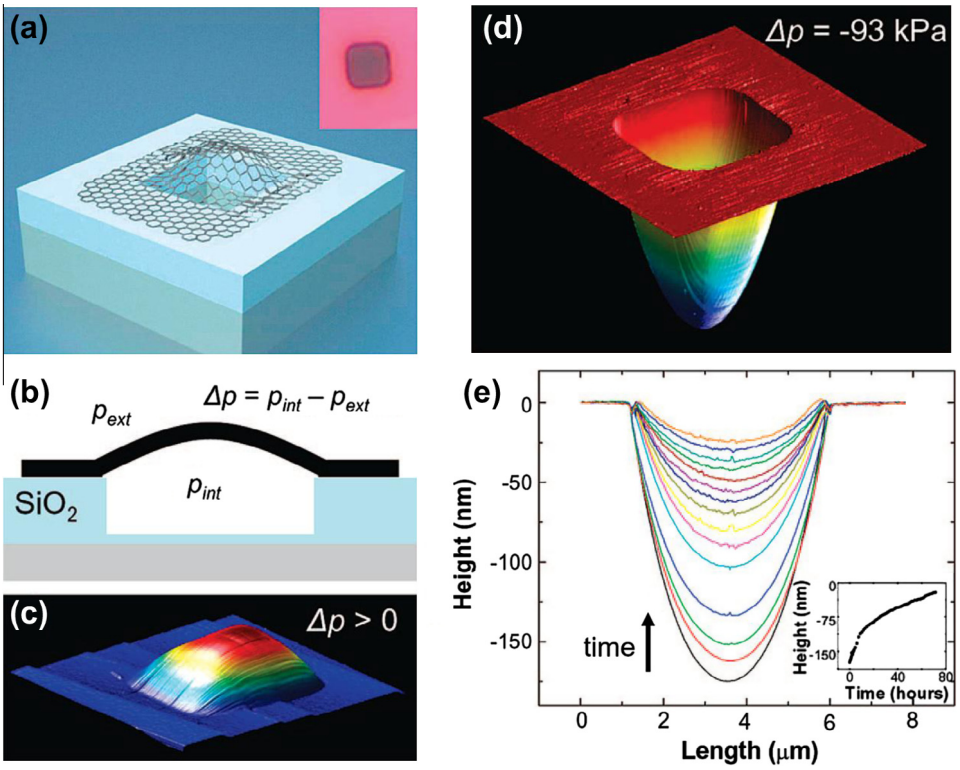

Fig. 2 – (a) Schematic of a graphene sealed microchamber. (Inset) optical image of a single atomic layer graphene drumhead on 440 nm of SiO_2. The dimensions of the microchamber are 4.75 × 4.75 μm × 380 nm. (b) Side view schematic of the graphene sealed microchamber. (c) Tapping mode atomic force microscope (AFM) image of a ~9 nm thick many layer graphene drumhead with $\Delta p > 0$. The dimensions of the square microchamber are 4.75 × 4.75 μm. The upward deflection at the center of the membrane is 90 nm. (d) AFM image of the graphene sealed microchamber of Fig. 1a with Δp −93 kPa across it. The minimum dip in the z direction is 175 nm. (e) AFM line traces taken through the center of the graphene membrane of (a). The images were taken continuously over a span of 71.3 h and in ambient conditions. (Inset) deflection at the center of the graphene membrane vs time. The first deflection measurement (z) 175 nm is taken 40 min after removing the microchamber from vacuum. From Ref. [4].

Please cite this article in press as: Berry V. Impermeability of graphene and its applications. Carbon (2013), http://dx.doi.org/10.1016/j.carbon.2013.05.052

a barrier of around 5.75–8 eV, 3–4 eV, 1–1.2 eV, 0.33–0.44, and 0.05–0.1 eV, respectively [38]. As will be discussed latter, the permeance of graphene can be controlled by opening fine pores in graphene.

3. Impermeable graphene microchambers for TEM imaging

Graphene presents an excellent opportunity to be employed as a material to encase liquid or wet samples for enhanced electron microscopy. The properties of graphene that make it ideal for fluid encasement for TEM imaging include: (a) impermeability [5,21] (as mentioned above), (b) high electron-transparency [22]: high-momentum electrons can transmit through monolayer or multilayer (1–10 nm) graphene, which enables facile TEM imaging, (c) flexibility [6,7] (which enables graphene to be rolled into carbon nanotubes) allows the sheets to conformally form chambers at nano-, micro- and macro- scale, (d) mechanical strength [5,23]: graphene's high yield-strength enables it to sustain the high pressure differences, similar to that between the fluidic region and external vacuum of a TEM, (e) high electrical conductivity [8,22]: the mobile π-electrons of graphene significantly reduce the electrostatic charge buildup under electron microscopy (EM), and (f) high thermal conductance [18]: graphene's high phonon-conductivity dissipates the heat generated from electron bombardment. Clearly, this unique combination of properties makes graphene an ideal nanomaterial for wet-phase imaging under TEM; while preserving volatile content under high vacuum.

These properties of graphene can be leveraged to image wet biological cells *via* electron microscopy [12,43]. For example, graphene functionalized with concanavalin – a pectin protein specifically binds to bacterial cell-wall (Gram positive) – can hermetically wrap the bacterial cells [12] (Fig. 3) and act as an impermeable, electron transparent encasement, allowing wet-imaging of the cells under TEM conditions (high vacuum) [2,44]. The graphene-wrapped bacteria's original shape, morphology and size from atmospheric pressure were retained under high vacuum TEM conditions. The mass transfer rate [35] from bacteria is given by:

$$\mathrm{MT} \propto \frac{k}{R} C_w + \frac{AI}{\lambda} C_w C_T \tag{3}$$

where k is the Darcian permeability, A is the electron-beam damage-factor, C_w and C_T are the water mass in and the total mass of a bacterium, R is the radius of the cell, I is the electron beam current and λ is the latent heat of vaporization. The initial rate of volume shrinkage is given by:

$$\left.\frac{dV}{dt}\right|_{t=0} = (V_{B0} + \alpha_1)\frac{\alpha_1\beta}{(1+\alpha_1)2} - \frac{\alpha_1\beta}{(1+\alpha_2)} = P^D \tag{4}$$

This provides combined permeability (P^D, Darcian and electron-beam induced permeability) where, V_{B0} is the volume fraction of completely dehydrated cell and α_1 and β are constants inversely proportional to membrane permeability, and α_2 is a constant proportional to the additional permeability caused by electron-beam induced membrane damage. Here, the Darcian permeability of cells reduces from 7.6 to 20 nm/s to practically zero for graphene wrapped cells. Therefore, this process can be used for cells to completely cut off the release of volatile material. The wrapping process cannot be used at higher temperature.

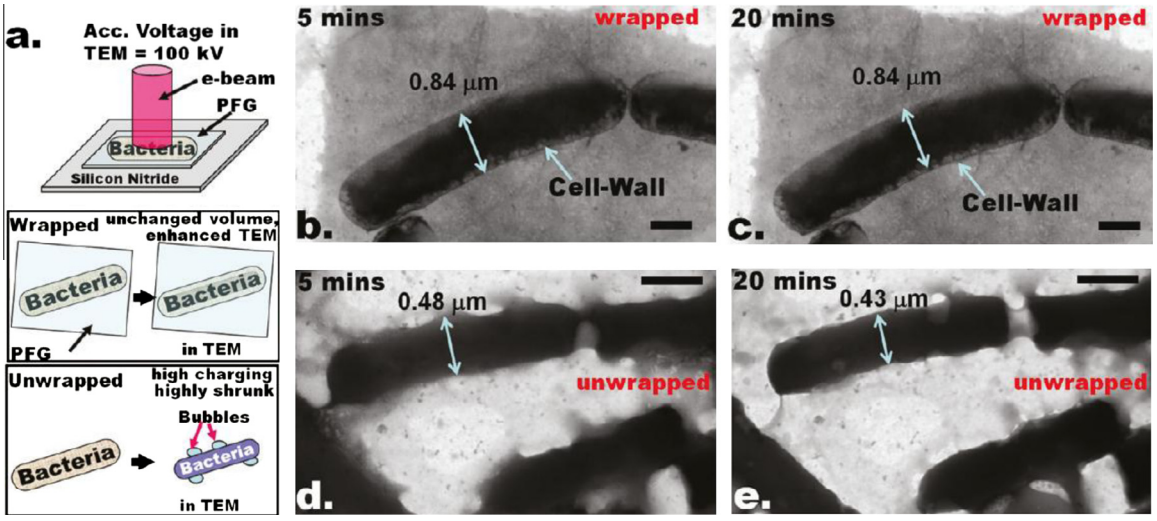

Fig. 3 – (a) Protein functionalized graphene (PFG) wrapping of bacteria prohibits shrinking under TEM. (b and c) Representative TEM images of wrapped bacterium (WB on 100 nm thick Si_3N_4 windows) exhibits no shrinkage from the original size after 5 and 20 min exposure. (d and e) Representative unwrapped bacteria (UWB) exhibit ~75% shrinkage after only 5 min under TEM vacuum (minimum time to obtain micrograph). Extensive bubbling is also observed during imaging, attributed to boiling of the volatile component of the cell's intracellular region (see videos in Supporting information). Scale bar = 500 nm. Note that under the same conditions, the cell wall of the wrapped bacteria is clearly discernible. This is attributed to significantly reduced charge accumulation due to the conductive PFGs (due to π-electrons). Further, it has been shown that graphene [7] and graphene oxide [10,11] can act as a great electron-transparent substrate for TEM imaging without the need for staining biological samples. From Ref. [12].

Please cite this article in press as: Berry V. Impermeability of graphene and its applications. Carbon (2013), http://dx.doi.org/10.1016/j.carbon.2013.05.052

The graphene encasement/wrapping mechanism on any substrate is a sequential multi-point attachment process, as favored by minimization of Gibbs energy:

$$\sum_{i=1}^{n}(\mu_{G+i}N_{G+i} + \mu_{B-i}N_{B-i}) > \sum_{i=1}^{n}(\mu_{GB\pm i}N_{GB\pm i}) \quad (5)$$

Here, μ is the chemical potential, N is the number of sites and the subscripts G+ and B− are the corresponding binding sites on graphene and substrate, respectively) [29]. Further, the sizeable reduction of free energy originating from the reduction of chemical potential *via* the highly-specific ligand–receptor interaction is expected to offset the ligand–receptor bond stretching during wrapping [29].

In 2011, *via* using a similar mechanism, Kempaiah et al. showed that yeast cells can also be wrapped with graphene oxide to provide a robust mechanical shell and electrically conductive surface [2] (Fig. 4). If the cells are not completely wrapped, they will leak out the intercellular volatile content, which leads to shrinkage of the yeast cell. As a result of the shrinkage of the cells, radial wrinkles form on graphene (1.5 nm thick) orthogonal to the boundary of the cell. The average wavelength of the wrinkles is given by: $\lambda = t(E/Es)^{1/3}$, where t is the thickness of graphene, E is the Young's modulus of graphene and Es is the Young's modulus of the cell wall. The calculated wrinkle wavelength of 20 nm matched with the experimental values of 40–70 nm, with the amplitude, A, of the wrinkles due to the in-plane shear estimated to be 28 nm ($A = (Lt/\lambda)[8/(3 + 3\nu)]^{1/2}$, [45] where ν is the Poisson ratio and L is the length of the cell). Therefore, wrapping the cells can provide both a route to image cells *via* electron microscope, or to create ordered wrinkles. More studies are required to understand the influence on the number of layers on the electron transparency of graphene for these applications.

Apart from imaging wet samples, graphene can enable observation of chemical processes in the liquid phase. In 2012, Yuk et al. [46] studied the growth on Pt nanocrystals in liquid phase at high resolution by creating a blister space between two graphene sheets, where aqueous solution of Pt cations was encased. This was followed by reduction of Pt cations by electron beam exposure at constant flux and their binding to form Pt nanocrystals. Here, graphene acted as an impermeable micro-chamber retaining the liquid phase, and an electron transparent membrane enabling electron-microscopy, while the liquid solution absorbed the electrons to reduce the Pt cations to nucleate the growth of nanocrystals of Pt. Therefore, it was possible to image the dynamics of growth of Pt nanocrystal in aqueous phase at high resolution via an aberration-corrected TEM; the monomer addition and coalescence events were directly observed. It is known that the nanocrystal growth is influenced by the interaction of the precursors with the chamber material. For example, in the case of silicon nitride encased TEM holders, the growth of the nanocrystals occurs near the wall. Interestingly, due to the low interaction of the Pt precursor and nanocrystal with graphene, the Pt nanocrystal growth in the graphene blister-chamber was independent of location, especially near the chamber-wall.

4. Impermeable graphene membranes as protective coating

Impermeable graphene can also be used as a barrier membrane for environmentally hazardous agents [47] and as an anti-corrosion coating [48]. In several chemical reactions, graphene acts as an inert material, where other materials undergo reaction. For anodic and cathodic scans on graphene coated nickel and copper, the current densities decreases by about an order of magnitude, and there is a sharp decrease in the reactions rates or reduction in ionic transfer. This implies that graphene acts as a protective layer to underlying metal. For Ni, the metallic ionization ($Ni \rightarrow Ni^{2+} + 2e$) and for Cu, cathodic reaction ($2H_2O + O_2 + 4e^- \rightarrow 4OH^-$) reduces implying low rate of corrosion. The corrosion current density for both metals reduces after graphene coating. For Ni the corrosion potential moves up by 0.3 V, while for Cu the corrosion potential reduces by 0.15 V [48–50].

Graphene oxide (GO) films also block the convective flow at a much lower loading in comparison to other carbon sources. For example, a film of GO (20 nm thick) coated on polyethylene membrane can reduce the permeability of toxic mercury vapors by 90% [47]. Here, at only 50 nm thickness, the hydrau-

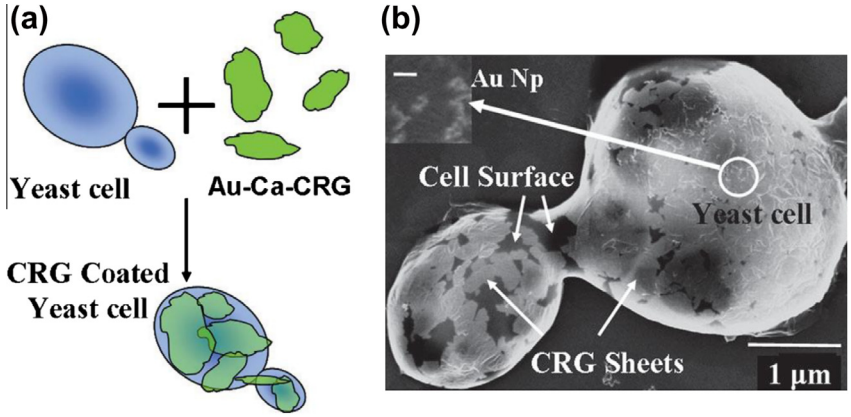

Fig. 4 – Interfacing of CRG sheets with SaC cells. (a) Schematic of the process where calcium ions are used to interface the CRG sheets with the SaC cells. (b) FESEM image shows the CRG sheets on the surface of the cells. They form a partial coverage on the surface. The inset shows the presence of the Au particles on the cell-CRG sheets. The scale is 50 nm. From Ref. [2].

Please cite this article in press as: Berry V. Impermeability of graphene and its applications. Carbon (2013), http://dx.doi.org/10.1016/j.carbon.2013.05.052

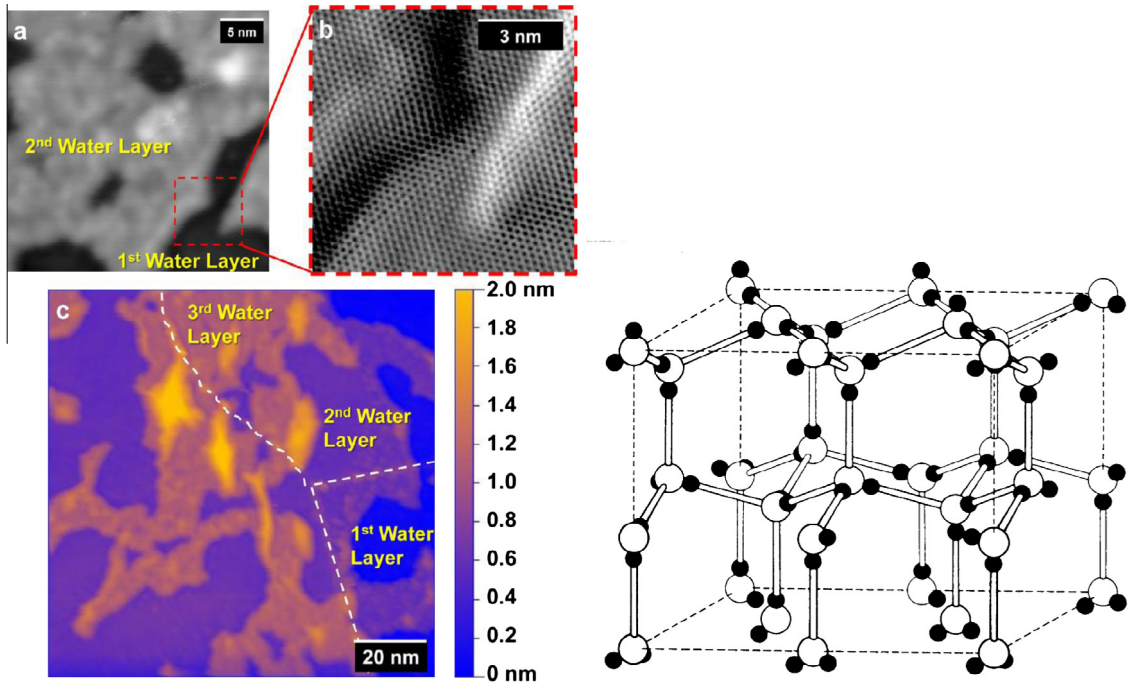

Fig. 5 – Scanning tunneling microscopy topographic scans of few layered water confined between graphene and mica. (a) Thrity nanometer by 30 nm image showing the first two water layers on the mica surface. (b) Zoomed-in spatial derivative of the boxed region in (a) showing the honeycomb lattice of the monolayer graphene coating. (c) Hundred nanometer by 100 nm false-colored topographic image of graphene–water–mica system. Three layers of water are visible, as well as a graphene grain boundary, which is labeled by the dotted white line. The protrusions coming out of the third water layer could be due to either contaminants trapped under the graphene or to the water displaying increasing bulklike properties as it gets further from the mica surface. Scanning conditions are −0.35 V sample bias and 1 nA tunneling current. The right panel shows the lattice structure of ice crystal. Adapted from Refs. [5,8]. (For interpretation of the references to colour in this figure legend, the reader is referred to the web version of this article.)

lic conductivity (for convective water flow) was measured to be 5×10^{-13} cm/s, which is lower than natural impervious materials such as granite and limestone. Therefore, graphene can function as an excellent protective coating for a large number of applications. Further, *via* microdroplet drying of GO with inorganic-nanostructures, an impermeable encasement of nanomaterials with GO forming a sack can be achieved [51]. This nanomaterial encased in GO can be used in environmental and biological applications where a physical barrier is important.

5. Stabilizing molecular monolayers

Water monolayers are known to be formed on mica surface under high humidity. Interestingly, impermeable graphene on mica can trap crystalline adlayers of water at room temperature. This allows accurate measure of the size of these adlayers on mica surface [52]. Several other studies have been used to understand the length scales of the water adsorbed on mica and other substrates, however the studies are challenging at room temperature due to the high vapor pressure of water. Graphene provides a highly conformal and flexible encasement, which can trap and retain the adlayers of water. An atomic force microscope (AFM) can then be used to measure the thickness of the water-adlayers. A puckered bilayer water from the structure of ice (Fig. 5) has a thickness of 0.369 nm, while that measured from graphene trapped water layers is 0.37 nm. This implies the crystalline formation of water adlayers similar to ice under graphene. Similarly, He et al. employed high-vacuum STM to study water layer between graphene and mica and found a height of 0.4 nm for first water later and additional 0.3 nm more for the next water layer [5] (Fig. 5). Therefore, impermeable graphene and its relative non-interaction with water enables imaging of water layer as a crystal[1] [8] (Fig. 5) on mica at room temperature. This is an important fundamental result made possible via the conformity and impermeability of graphene. Similar results are possible for other fluidic crystal-structures.

6. Graphene membranes for separation applications

Theoretical predictions suggest that artificial pores in graphene can increase its permeability and permeation-selectivity [39–41,44,53] (Fig. 6). For example, a nitrogen functionalized pore in graphene can open up an effective gap of 3 Å, which can lead to high selective diffusion of H_2 over CH_4 of 10^8; while a hydrogen terminated vacancy can open up 2.5 Å with

[1] http://www.benbest.com/cryonics/lessons.html

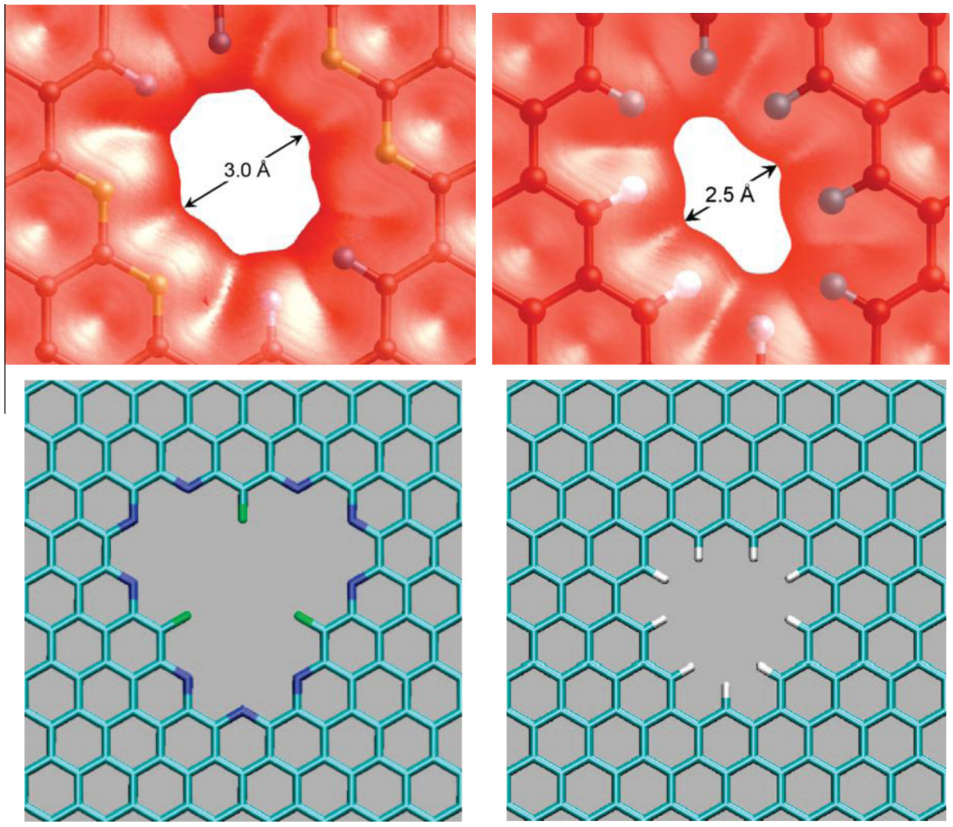

Fig. 6 – (Top) pore electron density iso-surface of (left) nitrogen functionalized and (right) hydrogen-terminated porous graphene (isovalue of 0.02 e/Å^3). (Bottom) functionalized graphene nanopores. (Left) the F–N-terminated nanopore. (Right) the H-terminated nanopore. Adapted from Refs. [1,6].

a selectivity of 10 [23] for H_2/CH_4 (Fig. 6) [1]. Similarly, periodic pores on graphene (two-dimensional polyphenylene networks [54,55]) can produce different barrier heights for transmission of different gases as well. For example, 2D polyphenylene theoretically exhibits a transmission barrier of 0.523, 1.245, and 4.832 eV for He, Ne, and CH_4 transport respectively [56]. These pores on graphene can be superior to the traditional polymeric or silica membranes [57] due to high permeance and selectivity.

Koenig et al. produced Angstrom scale pores on graphene blisters by controlled UV exposure (wavelengths of 185 nm and 254 nm) [58]. The UV-based etching rate is slow and thus produces small pores, unlike plasma based etching which is fast and challenging to control. The permeability was calculated by measuring the leak rate of the gases through the porous graphene blister. With pore sizes between 0.2 and 0.4 nm, a selectivity of $\sim 10^4$ between CH_4 and H_2 was achieved. Further, the diffusion of Ar remains unchanged before and after etching pores in graphene, implying complete blockage of Ar. The molecular diffusion rate through the pores was found to be inversely proportional to the size of the molecules.

There is also evidence of intrinsic pores in graphene produced via chemical vapor deposition, which is expected to have grain-boundaries and point defects. These were estimated to be between 1 and 14 nm [59]. Larger pores can be created by template etching in graphene *via* plasma [60]; however, those do not produce small enough pores to allow selective sieving. Therefore, a large number of possibilities exist to make porous graphene structures over a large range of pores.

Carbon nanotubes (CNTs) have also been used extensively in membrane applications; where, they can form two types of membranes: (a) randomly entangled CNT-paper structure where the molecules pass around CNTs and (b) isoporous membranes, where molecules pass through the interior of CNT tubes [61]. For the second type of CNT membranes, the collapsed vertically-aligned CNTs with no polymer show higher permeance (pore size = 3 nm) than CNT-membranes with polymer matrix [62]. Here, the flow of molecules through CNT exhibit varied levels of (frictionless) velocities, depending on the interaction of the molecule with the CNT walls [63,64]. Most importantly, the tip functionalization [65,66] can be used to control the flow of specific molecules through CNTs. For example, anionically charged CNT tip increased the diffusion of cationic molecules, an effect which reduces with increase in ionic concentration [66]. The molecular dynamics simulations have shown that while most molecules shows relatively frictionless motion thought the CNT, the chemistry of the tip of the CNT influences the selectivity [67].

7. Graphene pore ionic diffusion

Since atomically thick graphene is an impermeable membrane, a perfect graphene sheet separating two aqueous reservoirs of ions will not allow ionic trans-diffusion due to its

Please cite this article in press as: Berry V. Impermeability of graphene and its applications. Carbon (2013), http://dx.doi.org/10.1016/j.carbon.2013.05.052

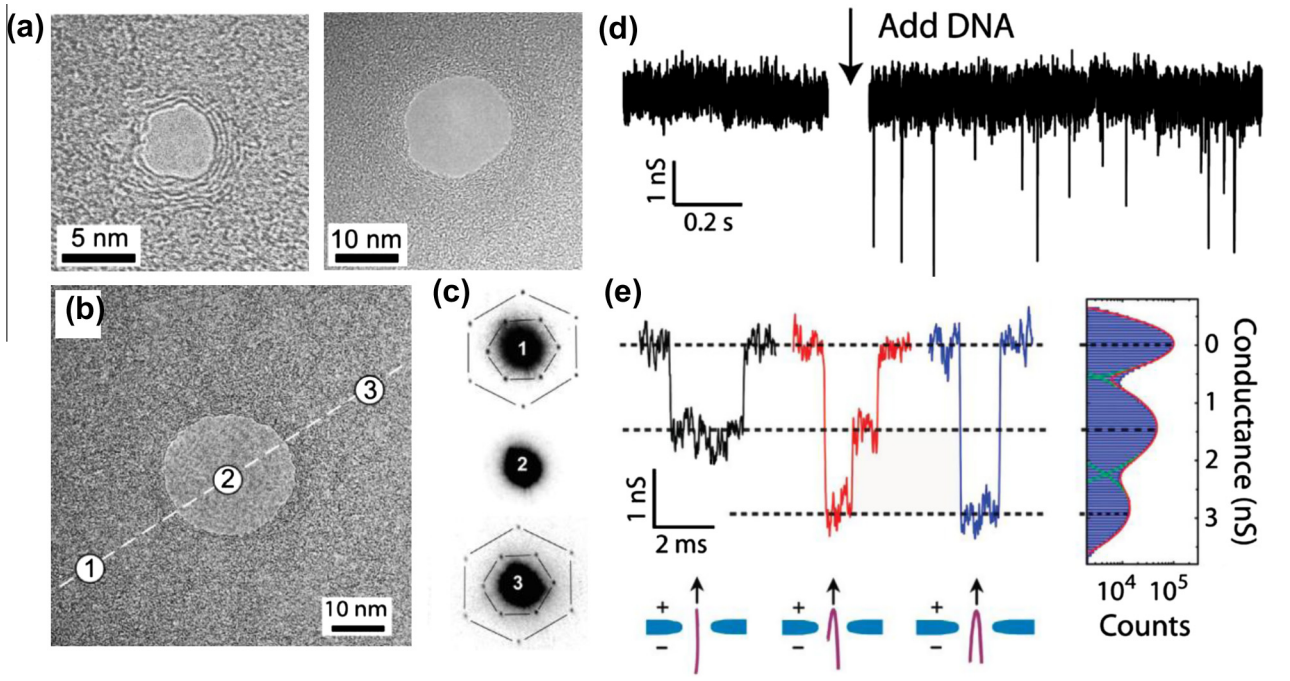

Fig. 7 – (a) Transmission electron microscopy (TEM) of nanopores drilled into multilayer graphene (b) TEM image of a 22 nm diameter pore in monolayer graphene. Incrusted numbers indicate spots where the diffraction patterns were recorded. (c) Diffraction patterns measured across the monolayer nanopore of panel left-b. (d–f) DNA translocation through a nanopore in a graphene monolayer. (d) Translocation of 48 kbp double-stranded λ-DNA across a 22 nm nanopore within a graphene monolayer, showing the baseline conductance and blockade events upon addition of DNA. (e) Examples of translocation events of nonfolded (black), partially folded (red), and fully folded (blue) DNA molecules recorded at 200 mV in the 22 nm pore. (f) Conductance histogram collected from 1222 translocation events, including the open-pore conductance before and after the event. Adapted from Ref. [3]. (For interpretation of the references to colour in this figure legend, the reader is referred to the web version of this article.)

impermeability [3]. However, a nanoscale pore in graphene will allow controlled trans-location (trans-diffusion) of ions [6] and long molecules such as DNA [3] via the pore from one side of graphene to the other (Figs. 6 and 7). With a 1 M KCl reservoir, the pore resistance scales with the pore-diameter: $R = \alpha/d^2$, with $\alpha = 2.4 \pm 0.2 \times 10^{-9}\ \Omega\ m^2$ [68]. Further, the chemical makeup of the pores influences the selectivity of the pores. For example, theoretical measurements show that H-, F- or N-terminated pores of 0.5 nm diameter in graphene can lead to selective ion diffusion. With a 0.1 V/nm, the F- and N-terminated pores allow only Li+, Na+ and K+ ions to pass, while H-terminated pore allows only F-, Cl- and Br-ions to pass. The selectivity is attributed to Coulomb coupling between ions and functional groups on graphene pores [6]. However, the selectivity-effect reduces with increase in the pore size.

It is important to note that the ions pass through a thin 0.3 nm thick graphene and in a short distance can translocate from one side to another. This is unlike solid-state-pores, where the thickness can be several nanometers. The modulation in the ionic currents [3] or lateral conductivity [69] can be used to detect the DNA or to read out the DNA sequence. For example, Schneider et al. has shown that the graphene nanopore could be used to determine the configuration of the DNA molecules passing through graphene nanopore at a higher resolution than the solid-state-nanopores [68] (Fig. 7). Again, this is because the solid-state nanopores are thicker than the dimensions of the DNA, while graphene has a compatible thickness to the DNA (Fig. 7). Therefore, the resolution at which the signal changes in graphene is much higher (0.3 nm). More work is required to realize the ability to sequence DNA as it passes through the nanopore.

8. Conclusion

Graphene is the most impermeable material owing to (a) the closed-spaced carbon atoms in graphene, (b) the high electron-density (π-cloud) which repels all molecules, (c) the high strength, and (d) its ultrathin (thinnest) structure. Since 2008 this property of graphene has been employed to develop several unprecedented applications, including (i) liquid encasements for wet electron microscopy, (ii) selective gas permeation, (iii) nanopore bio-diffusion, (iv) thinnest barrier against rusting [48,50], and (v) retention of molecular water layers. Futuristically, next generation impermeable-graphene systems could produce impermeable capsules, completely-sealed cages and gels [38], and answer some fundamental questions about fluidic chemical processes and structures. Along with a high strength, conductivity, and optical absorptivity, graphene's impermeability is set to open a wide range of exciting opportunities.

Please cite this article in press as: Berry V. Impermeability of graphene and its applications. Carbon (2013), http://dx.doi.org/10.1016/j.carbon.2013.05.052

Acknowledgment

VB thanks the financial support from NSF (CMMI-1054877, CMMI-0939523 and CMMI-1030963), Office of Naval Research (Grant N000141110767), Terry C. Johnson Center for Basic Cancer Research, and KSU start-up.

Appendix A. Supplementary data

Supplementary data associated with this article can be found, in the online version, at http://dx.doi.org/10.1016/j.carbon.2013.05.052.

REFERENCES

[1] Jiang D, Cooper VR, Dai S. Porous graphene as the ultimate membrane for gas separation. Nano Lett 2009;9(12):4019–24.
[2] Kempaiah R, Salgado S, Chung WL, Maheshwari V. Graphene as membrane for encapsulation of yeast cells: protective and electrically conducting. Chem Commun 2011;47(41):11480–2.
[3] Garaj S, Hubbard W, Reina A, Kong J, Branton D, Golovchenko JA. Graphene as a subnanometre trans-electrode membrane. Nature 2010;467(7312):190–3.
[4] Bunch JS, Verbridge SS, Alden JS, van der Zande AM, Parpia JM, Craighead HG, et al. Impermeable atomic membranes from graphene sheets. Nano Lett 2008;8(8):2458–62.
[5] He KT, Wood JD, Doidge GP, Pop E, Lyding JW. Scanning tunneling microscopy study and nanomanipulation of graphene-coated water on mica. Nano Lett 2012;12(6):2665–72.
[6] Sint K, Wang B, Kra¦ül P. Selective ion passage through functionalized graphene nanopores. J Am Chem Soc 2008;130(49):16448–9.
[7] Nair RR, Blake P, Blake JR, Zan R, Anissimova S, Bangert U, et al. Graphene as a transparent conductive support for studying biological molecules by transmission electron microscopy. Appl Phys Lett 2010;97(15):153102.
[8] http://www.benbest.com/cryonics/lessons.html.
[9] Novoselov KS, Geim AK, Morozov SV, Jiang D, Zhang Y, Dubonos SV, et al. Electric field effect in atomically thin carbon films. Science 2004;306(5296):666–9.
[10] Wilson NR, Pandey PA, Beanland R, Young RJ, Kinloch IA, Gong L, et al. Graphene oxide: structural analysis and application as a highly transparent support for electron microscopy. ACS Nano 2009;3(9):2547–56.
[11] Riedl C, Zakharov AA, Starke U. Precise in situ thickness analysis of epitaxial graphene layers on SiC(0001) using low-energy electron diffraction and angle resolved ultraviolet photoelectron spectroscopy. Appl Phys Lett 2008;93(3):033106.
[12] Mohanty N, Fahrenholtz M, Nagaraja A, Boyle D, Berry V. Impermeable graphenic encasement of bacteria. Nano Lett 2011;11(3):1270–5.
[13] Gass MH, Bangert U, Bleloch AL, Wang P, Nair RR, Geim AK. Free-standing graphene at atomic resolution. Nat Nanotechnol 2008;3(11):676–81.
[14] Du X, Skachko I, Barker A, Andrei EY. Approaching ballistic transport in suspended graphene. Nat Nanotechnol 2008;3(8):491–5.
[15] Chen JH, Jang C, Xiao SD, Ishigami M, Fuhrer MS. Intrinsic and extrinsic performance limits of graphene devices on SiO_2. Nat Nanotechnol 2008;3(4):206–9.
[16] Akturk A, Goldsman N. Electron transport and full-band electron–phonon interactions in graphene. J Appl Phys 2008;103:053702.
[17] Nair RR, Blake P, Grigorenko AN, Novoselov KS, Booth TJ, Stauber T, et al. Fine structure constant defines visual transparency of graphene. Science 2008;320(5881):1308.
[18] Balandin AA, Ghosh S, Bao W, Calizo I, Teweldebrhan D, Miao F, et al. Superior thermal conductivity of single-layer graphene. Nano Lett 2008;8(3):902–7.
[19] Lee C, Wei XD, Kysar JW, Hone J. Measurement of the elastic properties and intrinsic strength of monolayer graphene. Science 2008;321(5887):385–8.
[20] Xia F, Mueller T, Lin Y, Valdes-Garcia A, Avouris P. Ultrafast graphene photodetector. Nat Nanotechnol 2009;4(12):839–43.
[21] Schedin F, Geim AK, Morozov SV, Hill EW, Blake P, Katsnelson MI, et al. Detection of individual gas molecules adsorbed on graphene. Nat Mater 2007;6(9):652–5.
[22] Lu GH, Ocola LE, Chen JH. Gas detection using low-temperature reduced graphene oxide sheets. Appl Phys Lett 2009;94(8):083111.
[23] Avouris P, Chen ZH, Perebeinos V. Carbon-based electronics. Nat Nanotechnol 2007;2(10):605–15.
[24] Dawlaty JM, Shivaraman S, Chandrashekhar M, Rana F, Spencer MG. Measurement of ultrafast carrier dynamics in epitaxial graphene. Appl Phys Lett 2008;92:042116.
[25] Lin YM, Jenkins KA, Valdes-Garcia A, Small JP, Farmer DB, Avouris P. Operation of graphene transistors at gigahertz frequencies. Nano Lett 2009;9(1):422–6.
[26] Mohanty N, Berry V. Graphene-based single-bacterium resolution biodevice and DNA transistor: interfacing graphene derivatives with nanoscale and microscale biocomponents. Nano Lett 2008;8(12):4469–76.
[27] Meyer JC, Girit CO, Crommie MF, Zettl A. Imaging and dynamics of light atoms and molecules on graphene. Nature 2008;454(7202):319–22.
[28] Abanin DA, Lee PA, Levitov LS. Charge and spin transport at the quantum hall edge of graphene. Solid State Commun 2007;143(1–2):77–85.
[29] Shen T, Wu YQ, Capano MA, Rokhinson LP, Engel LW, Ye PD. Magnetoconductance oscillations in graphene antidot arrays. Appl Phys Lett 2008;93(12):122102.
[30] Semenov YG, Kim KW, Zavada JM. Spin field effect transistor with a graphene channel. Appl Phys Lett 2007;91(15):153105.
[31] Novoselov KS, Geim AK, Morozov SV, Jiang D, Katsnelson MI, Grigorieva IV, et al. Two-dimensional gas of massless Dirac fermions in graphene. Nature 2005;438(7065):197–200.
[32] Novoselov KS, Jiang D, Schedin F, Booth TJ, Khotkevich VV, Morozov SV, et al. Two-dimensional atomic crystals. Proc Natl Acad Sci USA 2005;102(30):10451–3.
[33] Gilje S, Han S, Wang M, Wang KL, Kaner RB. A chemical route to graphene for device applications. Nano Lett 2007;7(11):3394–8.
[34] Gomez-Navarro C, Weitz RT, Bittner AM, Scolari M, Mews A, Burghard M, et al. Electronic transport properties of individual chemically reduced graphene oxide sheets. Nano Lett 2007;7(11):3499–503.
[35] Barone V, Hod O, Scuseria GE. Electronic structure and stability of semiconducting graphene nanoribbons. Nano Lett 2006;6(12):2748–54.
[36] Sreeprasad TS, Berry V. How do the electrical properties of graphene change with its functionalization? Small 2012;9:341–50.
[37] Koenig SP, Boddeti NG, Dunn ML, Bunch JS. Ultrastrong adhesion of graphene membranes. Nat Nanotechnol 2011;6(9):543–6.
[38] Leenaerts O, Partoens B, Peeters FM. Graphene: a perfect nanoballoon. Appl Phys Lett 2008;93(19):193107.
[39] Hrusak J, Bohme DK, Weiske T, Schwarz H. Ab initio MO calculation on the energy barrier for the penetration of a benzene ring by a helium atom. Model studies for the formation of endohedral He@C60+ complexes by

high-energy bimolecular reactions. Chem Phys Lett 1992;193(1–3):97–100.
[40] Murry RL, Scuseria GE. Theoretical evidence for a C60 "window" mechanism. Science 1994;263(5148):791–3.
[41] Geim AK, Novoselov KS. The rise of graphene. Nat Mater 2007;6(3):183–91.
[42] Georgiou T, Britnell L, Blake P, Gorbachev RV, Gholinia A, Geim AK, et al. Graphene bubbles with controllable curvature. Appl Phys Lett 2011;99(9):093103.
[43] Nguyen P, Berry V. Graphene interfaced with biological cells: opportunities and challenges. J Phys Chem Lett 2012;3(8):1024–9.
[44] Lee Z, Jeon KJ, Dato A, Erni R, Richardson TJ, Frenklach M, et al. Direct imaging of soft–hard interfaces enabled by graphene. Nano Lett 2009;9(9):3365–9.
[45] Bao W, Miao F, Chen Z, Zhang H, Jang W, Dames C, et al. Controlled ripple texturing of suspended graphene and ultrathin graphite membranes. Nat Nanotechnol 2009;4(9):562–6.
[46] Yuk JM, Park J, Ercius P, Kim K, Hellebusch DJ, Crommie MF, et al. High-resolution EM of colloidal nanocrystal growth using graphene liquid cells. Science 2012;336(6077):61–4.
[47] Guo F, Silverberg G, Bowers S, Kim SP, Datta D, Shenoy V, et al. Graphene-based environmental barriers. Environ Sci Technol 2012;46(14):7717–24.
[48] Kirkland NT, Schiller T, Medhekar N, Birbilis N. Exploring graphene as a corrosion protection barrier. Corros Sci 2012;56:1–4.
[49] Singh Raman RK, Chakraborty Banerjee P, Lobo DE, Gullapalli H, Sumandasa M, Kumar A, et al. Protecting copper from electrochemical degradation by graphene coating. Carbon 2012;50(11):4040–5.
[50] Prasai D, Tuberquia JC, Harl RR, Jennings GK, Bolotin KI. Graphene: corrosion-inhibiting coating. Acs Nano 2012;6(2):1102–8.
[51] Chen Y, Guo F, Jachak A, Kim SP, Datta D, Liu J, et al. Aerosol synthesis of cargo-filled graphene nanosacks. Nano Lett 2012;12(4):1996–2002.
[52] Xu K, Cao P, Heath JR. Graphene visualizes the first water adlayers on mica at ambient conditions. Science 2010;329(5996):1188–91.
[53] Suk ME, Aluru NR. Water transport through ultrathin graphene. J Phys Chem Lett 2010;1(10):1590–4.
[54] Bieri M, Treier M, Cai J, It-Mansour K, Ruffieux P, Groning O, et al. Porous graphenes: two-dimensional polymer synthesis with atomic precision. Chem Commun 2009:6919–21.
[55] Li Y, Zhou Z, Shen P, Chen Z. Two-dimensional polyphenylene: experimentally available porous graphene as a hydrogen purification membrane. Chem Commun 2010;46(21):3672–4.
[56] Schrier J. Helium separation using porous graphene membranes. J Phys Chem Lett 2010;1(15):2284–7.
[57] Du H, Li J, Zhang J, Su G, Li X, Zhao Y. Separation of hydrogen and nitrogen gases with porous graphene membrane. J Phys Chem C 2011;115(47):23261–6.
[58] Koenig SP, Wang L, Pellegrino J, Bunch JS. Selective molecular sieving through porous graphene. Nat Nanotechnol 2012;7:724–32.
[59] OΓÇÖHern SC, Stewart CA, Boutilier MSH, Idrobo JC, Bhaviripudi S, Das SK, et al. Selective molecular transport through intrinsic defects in a single layer of CVD graphene. Acs Nano 2012;6(11):10130–8.
[60] Zeng Z, Huang X, Yin Z, Li H, Chen Y, Li H, et al. Fabrication of graphene nanomesh by using an anodic aluminum oxide membrane as a template. Adv Mater 2012;24(30):4138–42.
[61] Sears K, Dume L, Schtz J, She M, Huynh C, Hawkins S, et al. Recent developments in carbon nanotube membranes for water purification and gas separation. Materials 2010;3(1):127–49.
[62] Yu M, Funke HH, Falconer JL, Noble RD. High density, vertically-aligned carbon nanotube membranes. Nano Lett 2008;9(1):225–9.
[63] Majumder M, Chopra N, Andrews R, Hinds BJ. Nanoscale hydrodynamics: enhanced flow in carbon nanotubes. Nature 2005;438(7064):44.
[64] Sun L, Crooks RM. Single carbon nanotube membranes: a well-defined model for studying mass transport through nanoporous materials. J Am Chem Soc 2000;122(49):12340–5.
[65] Hinds BJ, Chopra N, Rantell T, Andrews R, Gavalas V, Bachas LG. Aligned multiwalled carbon nanotube membranes. Science 2004;303(5654):62–5.
[66] Majumder M, Chopra N, Hinds BJ. Effect of tip functionalization on transport through vertically oriented carbon nanotube membranes. J Am Chem Soc 2005;127(25):9062–70.
[67] Kalra A, Garde S, Hummer G. Osmotic water transport through carbon nanotube membranes. Proc Natl Acad Sci USA 2003;100(18):10175–80.
[68] Schneider GF, Kowalczyk SW, Calado VE, Pandraud G, Zandbergen HW, Vandersypen LM, et al. DNA translocation through graphene nanopores. Nano Lett 2010;10(8):3163–7.
[69] Nelson T, Zhang B, Prezhdo OV. Detection of nucleic acids with graphene nanopores: ab initio characterization of a novel sequencing device. Nano Lett 2010;10:3237–42.

Please cite this article in press as: Berry V. Impermeability of graphene and its applications. Carbon (2013), http://dx.doi.org/10.1016/j.carbon.2013.05.052